Journal of Sound and Vibration 329 (2010) 3691–3708

Contents lists available at ScienceDirect

Journal of Sound and Vibration

journal homepage: www.elsevier.com/locate/jsvi

Identification of source velocities on 3D structures in non-anechoic environments: Theoretical background and experimental validation of the inverse patch transfer functions method

M. Aucejo *, N. Totaro, J.-L. Guyader

Laboratoire Vibrations Acoustique, INSA Lyon, 25 bis avenue Jean Capelle 69621, Villeurbanne Cedex, France

ARTICLE INFO

Article history:
Received 12 November 2008
Received in revised form
11 March 2010
Accepted 29 March 2010
Handling Editor: Y. Auregan

ABSTRACT

In noise control, identification of the source velocity field remains a major problem open to investigation. Consequently, methods such as nearfield acoustical holography (NAH), principal source projection, the inverse frequency response function and hybrid NAH have been developed. However, these methods require free field conditions that are often difficult to achieve in practice. This article presents an alternative method known as inverse patch transfer functions, designed to identify source velocities and developed in the framework of the European SILENCE project. This method is based on the definition of a virtual cavity, the double measurement of the pressure and particle velocity fields on the aperture surfaces of this volume, divided into elementary areas called patches and the inversion of impedances matrices, numerically computed from a modal basis obtained by FEM. Theoretically, the method is applicable to sources with complex 3D geometries and measurements can be carried out in a non-anechoic environment even in the presence of other stationary sources outside the virtual cavity. In the present paper, the theoretical background of the iPTF method is described and the results (numerical and experimental) for a source with simple geometry (two baffled pistons driven in antiphase) are presented and discussed.

1. Introduction

Nearfield acoustical holography (NAH), first introduced by Williams et al. [1,2], is based on the 2D Fourier Transform of the complex pressure field at a given frequency measured on a hologram near the source. Measurements of the pressure field are generally made on a plane surface and make possible the determination of the 3D source velocity field. However, NAH is mainly applicable to simple geometries (planes [3], cylinders [4] and spheres [5]). Furthermore, problems of discontinuities exist at boundaries due to the lack of information beyond the measurement zone, though information is nevertheless necessary in order to compute the 2D Fourier Transform. Thus measurements have to be made in the acoustical nearfield of the structure to avoid the influence of boundary effects.

The inverse frequency response function method is based on the evaluation and inversion of transfer matrices that can be obtained either experimentally or numerically. In the latter case, if the computation of the transfer functions is based on the boundary element method, it is called iBEM. This method can be used to reconstruct acoustic radiation on arbitrary surfaces [6]. Martinus [7] uses this method to determine the distribution of particle velocity on the open end of a

* Corresponding author. Fax: +33 4 72 43 87 12.
E-mail address: mathieu.aucejo@insa-lyon.fr (M. Aucejo).

0022-460X/$ - see front matter © 2010 Elsevier Ltd. All rights reserved.
doi:10.1016/j.jsv.2010.03.032

rectangular duct and shows that sound pressure field measurements do not have to be made in the nearfield of the source to obtain good results. However, the main drawback of iBEM is that it demands an excessive number of measurements to determine the acoustic field on a complex structure, since it requires a fine mesh definition (six nodes per wavelength). The difficulty of the method also stems from the inversion of the transfer matrices, which are often ill-conditioned and thus require the use of regularization methods.

Other methods have also been developed to overcome the difficulties and limitations inherent to NAH and iBEM. Thus a hybrid NAH was introduced [8,9] based on a modified HELS (Helmholtz equation least squares) method [10,11]. It allows reconstructing the pressure field on a complex shaped surface very close to the source surface. As with NAH applications, hybrid NAH requires regularization, due to measurement uncertainty and the incompleteness of the acoustic pressure field leading to ill-conditioned transfer matrices. Furthermore, the modified HELS method can also be combined with iBEM [12] to reconstruct acoustic quantities on a virtual sphere enclosing the source structure, possibly leading to the loss of nearfield information. Finally, to avoid large numbers of measurements, the principal source projection method was developed [13,14]. This method is based on the evaluation of a radiation operator between the source surface, represented by a distribution of elementary sources, and a grid of measurements. In traditional methods like iBEM, the number of identified acoustic sources is limited to the number of microphones in order to guarantee the uniqueness of the solution. On the contrary, for the principal source projection method, the number of quantified sources is higher than the number of microphones, which means that the system is under-determined. In addition, to identify the data on the source surface, the transfer functions, calculated between a point of the elementary source and a measurement point, have to be inverted. The transfer matrix is often ill-conditioned, which implies the use of regularization methods such as truncated singular value decomposition.

In this article, an alternative method, i.e. the iPTF method, is introduced to identify source velocities. This method is derived from the patch transfer functions (PTF) method [15–17]. In its direct formulation, the PTF method is a tool used to predict pressure inside and outside a cavity containing acoustic sources and apertures by relying on substructuring and impedance concepts. The acoustical medium is divided into subdomains and PTFs are evaluated by suitable methods for each subdomain (FEM, Rayleigh approach, measurements, …). Subdomains are then coupled through their common surface and divided into patches. Coupling conditions are written for each patch as pressure and velocity equations, describing the local equilibrium. A system of linear equations is finally obtained, where the unknowns are coupling patch velocities. The system is solved to determine the coupling velocities and finally the pressures at any point of the acoustical domain.

The aim of the inverse approach (iPTF method) is to determine source velocities from patch pressures and velocities measured on boundaries of a virtual cavity. Theoretically, the iPTF method allows identifying source velocities in a noisy environment (i.e. in the presence of other sources) by the replicated measurement of the pressure and particle velocity fields on a surface surrounding the source. This is not possible with classical methods as they only use sound pressure measurements. Measurements can thus be made, for instance, on a part of an engine in operation. However, as classically observed in inverse methods, the inversion of an ill-conditioned matrix is required. However, this drawback can be bypassed by using suitable regularization techniques such as truncated singular value decomposition or that proposed by Tikhonov. Finally, one of the advantages of the iPTF method is the use of the finite element method (FEM) as a solver. Whereas other methods require analytical or BEM models to estimate transfer functions, iPTF only requires the modal basis of a virtual cavity to compute Patch Transfer Functions. This makes the method applicable even to sources with complex geometries.

The present article deals with the theoretical background of the method and its numerical and experimental application to a simple case (two baffled pistons driven in antiphase). This test case is voluntarily simplified in order to facilitate the study of the main features of the method proposed, namely the size of the virtual cavity, the number of measurement patches, the ability to localize and separate sources and finally the robustness of the method with respect to an external stationary disturbing source. Experimental validations of the iPTF approach confirm the expected advantages and demonstrate the applicability of the method.

2. Theoretical background of the iPTF method

2.1. Basic concept of the iPTF method: the integral formulation

Let us consider the acoustic cavity Ω presented in Fig. 1. The acoustical domain Ω is delimited by a rigid surface S_r, an absorbing surface S_a, a vibrating surface S_v and a surface with Dirichlet conditions S_d. Furthermore, an acoustic source S_0 is located inside the acoustic cavity Ω, but outside the volume Ω_c. Consequently, the problem to be solved is expressed by

$$\begin{cases} \Delta p(M)+k^2 p(M)=S_0(M), & \forall M\in\Omega,\\ \dfrac{\partial p}{\partial n}(Q)=0, & \forall Q\in S_r,\\ \dfrac{\partial p}{\partial n}(Q)=-\mathrm{j}\rho\omega V(Q), & \forall Q\in S_v,\\ p(Q)=p_0, & \forall Q\in S_d,\\ p(Q)=-\dfrac{Z}{\mathrm{j}\rho\omega}\dfrac{\partial p}{\partial n}(Q), & \forall Q\in S_a, \end{cases} \tag{1}$$

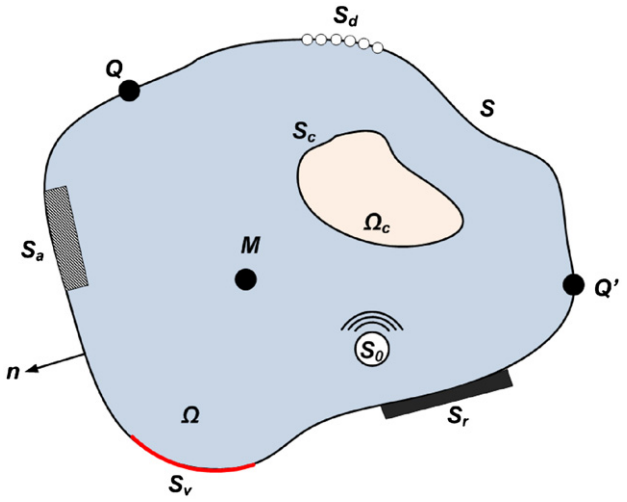

Fig. 1. Integral problem.

where Δ is the Laplacian operator, $\partial/\partial n$ the normal derivative outwardly directed, ρ the density of air, $V(Q)$ the normal velocity imposed on S_v, p_0 the pressure imposed on S_d, Z the surface impedance of the absorbing material, ω the angular frequency and k the acoustic wavenumber.

Now, let us write Green's identity applied to the volume $\Omega_c \subset \Omega$,

$$\iiint_{\Omega_c} (\Psi\Delta\Phi - \Phi\Delta\Psi)\,\mathrm{d}\Omega_c = \iint_{S_c} \left(\Phi\frac{\partial\Psi}{\partial n} - \Psi\frac{\partial\Phi}{\partial n}\right)\mathrm{d}S_c. \tag{2}$$

The previous expression is very general and functions Φ and Ψ are arbitrary. In the present work, we first assume that function Φ is the acoustic pressure p. In the volume Ω_c, the pressure satisfies the homogeneous Helmholtz equation as expressed in

$$\Delta p(M) + k^2 p(M) = 0, \quad \forall M \in \Omega_c. \tag{3}$$

The function Ψ is chosen as a particular Green's function G satisfying the homogeneous Neumann's problem for a point Q' located on the boundary surface S_c as expressed in

$$\begin{cases} \Delta G(M,Q') + k^2 G(M,Q') = \delta(M-Q'), & \forall M \in \Omega_c,\ Q' \in S_c, \\ -\dfrac{1}{\mathrm{j}\rho\omega}\dfrac{\partial G}{\partial n}(Q,Q') = 0, & \forall Q \in S_c. \end{cases} \tag{4}$$

Introducing Eqs. (3) and (4) in Eq. (2), we finally obtain the integral equation given by

$$p(Q') = \iint_{S_c} G(Q,Q')\frac{\partial p}{\partial n}(Q)\,\mathrm{d}Q. \tag{5}$$

When using Euler's equation in Eq. (5), the acoustic pressure $p(Q')$ at point Q' is related to normal velocity $V_n(Q)$ at each point Q of surface S_c as expressed

$$p(Q') = -\mathrm{j}\rho\omega \iint_{S_c} G(Q,Q')V_n(Q)\,\mathrm{d}Q. \tag{6}$$

The Green's function used is that of a virtual cavity whose boundary surface S_c is assumed to be rigid. It is important to note that these rigid wall boundary conditions have no physical reality. They exist only to provide a mathematical tool for solving the virtual cavity problem.

Finally, the key point of this formulation is that external sources located outside the cavity do not modify the integral equation. In other words, this formulation is independent of acoustic sources external to Ω_c.

2.2. Basic equation of the iPTF method

Let us consider the practical situation given in Fig. 2, where a virtual cavity of surface $S_c = S_m \cup S_v$ surrounds the source and separates the acoustical domain into a virtual cavity Ω_c and an external domain Ω_e.

The numerical solution of the previous integral equation is based on the discretization of surface S_c into N elementary areas A_r called patches. The discretization of Eq. (6) into patches leads to Eq. (7), describing the relation between the space average normal velocity $\overline{v}_r$ on patch r and the space average pressure $\overline{p}_j$ on patch j. It should be noted that this relation

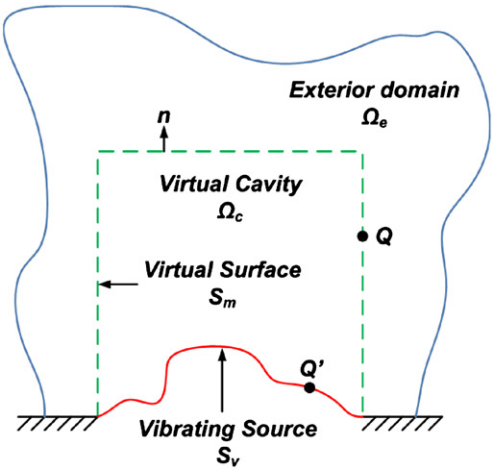

Fig. 2. Basic identification problem.

remains true provided that the size of the patches is small compared to the acoustic wavelength.

$$\overline{p}_j = \sum_{r=1}^{N} Z_{jr}\overline{v}_r. \tag{7}$$

In Eq. (7), the space average pressure and velocity are related by the patch impedance Z_{jr}. Consequently, the patch impedance Z_{jr} between the excited patch r and the receiving patch j is defined as the ratio of the space average pressure $\overline{p}_{jr}$ on a patch j and the space average normal velocity $\overline{v}_r$ on a patch r as expressed in

$$Z_{jr} = \frac{\overline{p}_{jr}}{\overline{v}_r}, \tag{8}$$

where the space average is defined as $\bar{\cdot}_r = 1/A_r \int_{A_r} \cdot \, \mathrm{d}A_r$.

The basic equation of the iPTF is derived from Eq. (7), where the contribution of patches is separated into patches belonging to source surface S_v and patches belonging virtual surface S_m as expressed by

$$\overline{p}_j = \sum_{k=1}^{P} Z_{jk}\overline{v}_k + \sum_{i=1}^{M} Z_{ji}\overline{v}_i, \tag{9}$$

where j and i belong to S_m, k belongs to S_v and $N=M+P$.

Now, the iPTF formulation can be obtained from Eq. (9) in a straightforward manner. For the sake of simplicity, Eq. (9) is written in matrix form and the following notations are considered: $P_j = \overline{p}_j$, $V_i = \overline{v}_i$ and $V_k = \overline{v}_k$.

$$\{P_j\} = [Z_{jk}]\{V_k\} + [Z_{ji}]\{V_i\}. \tag{10}$$

It should be noted that in matrices $[Z_{ji}]$ and $[Z_{jk}]$, the number of lines j represents the number of patch pressure measurements $\{P_j\}$, while the number of columns k corresponds to the number of identification patches of source velocity $\{V_k\}$ and i represents the number of patch velocity measurements $\{V_i\}$.

The vector of source velocities $\{V_k\}$ is thus easily obtained after simple matrix manipulation and is the basic equation of the iPTF method,

$$\{V_k\} = [Z_{jk}]^{-1}(\{P_j\} - [Z_{ji}]\{V_i\}). \tag{11}$$

Insofar as the impedance matrices $[Z_{jk}]$ and $[Z_{ji}]$ are computed numerically, only pressures $\{P_j\}$ and velocities $\{V_i\}$ have to be measured on each patch of the virtual surface S_m to calculate the mean patch source velocities $\{V_k\}$. In the iPTF method, patch pressure $\{P_j\}$ and patch velocity $\{V_i\}$ are measured with pressure–velocity (PU) probes. These PU probes have been assessed by Jacobsen and Jaud [18,19]. One important point is that the velocity field on the virtual surface can be due to the direct field from the vibrating surface as well as sound reflected by obstacles placed outside the virtual cavity. Thus this method is not restricted to the anechoic environment and is theoretically independent of sources located outside the measurement area by virtue of the Kirchhoff's integral. Nevertheless, the inversion of the impedances matrices can be difficult, since these matrices are rectangular and ill-conditioned as is presented in the Section 2.4.

2.3. Computation of patch impedance Z_{jr}

As already mentioned in Section 2.2, the patch impedance matrices $[Z_{jk}]$ and $[Z_{ji}]$ are computed numerically. They are derived from the integral formulation (see Eq. (6)) and the expansion on virtual rigid wall cavity modes. To obtain these

quantities, it is necessary to calculate function $G(Q,Q')$ satisfying Eq. (4). To do this, we expand the solution on the normal modes of the rigid wall cavity. This leads to the Green's function given by Eq. (12). In Appendix A, the detailed calculation of Green's function is presented.

$$G(Q,Q') = \sum_n \frac{c^2 \phi_n(Q)\phi_n(Q')}{\Lambda_n(\omega_n^2 - \omega^2 + j\eta_n\omega_n\omega)}, \tag{12}$$

where Λ_n is the norm of the mode n, η_n the modal damping, avoiding singularities when $\omega = \omega_n$.

Then, the pressure $p(Q')$ created by a constant normal velocity $\overline{v}_r$ imposed on a patch r of surface S_r can be calculated from

$$p(Q') = -j\rho\omega c^2 S_r \sum_n \frac{\overline{\phi}_{n_r}\phi_n(Q')}{\Lambda_n(\omega_n^2 - \omega^2 + j\eta_n\omega_n\omega)}\overline{v}_r. \tag{13}$$

The patch impedance Z_{jr} between the excited patch r and the receiving patch j is therefore given by Eq. (14), where the space average pressure over the receiving patches is introduced:

$$Z_{jr} = \frac{\overline{p}_{jr}}{\overline{v}_r} = -\sum_n \frac{j\omega\rho c^2 S_r}{\Lambda_n(\omega_n^2 - \omega^2 + j\eta_n\omega_n\omega)}\overline{\phi_{n_r}}\,\overline{\phi_{n_j}}. \tag{14}$$

It can be seen that the natural frequencies ω_n and the mode shapes of the virtual rigid wall cavity ϕ_n are obtained by FE calculation, which permits dealing with complex source geometries.

2.4. Explanations of ill-conditioned impedance matrices

In the iPTF method, impedance matrix $[Z_{jk}]$ has to be inverted. However, this matrix can be ill-conditioned. Consequently, it is important to identify factors causing the ill-conditioning of matrix $[Z_{jk}]$. To achieve this, the conditioning number κ is a good indicator and serves as the basis for the following discussion. The conditioning number is defined in this article as the ratio between the biggest singular value σ_1 of $[Z_{jk}]$ and the smallest one σ_n as expressed by

$$\kappa(Z_{jk}) = \frac{\sigma_1}{\sigma_n}. \tag{15}$$

It should be recalled that matrix $[Z_{jk}]$ describes the relation between the number of patches j, where patch pressures $\{P_j\}$ are measured and the number of patches k, where patch source velocities $\{V_k\}$ are identified.

2.4.1. Influence of pressure information on the source surface

Let us consider the source surface presented in Fig. 3. To avoid particular cases, this source surface has no symmetries. A virtual cavity is then defined as are the measurement and source patch meshes, as shown in Fig. 3. The dimensions of the virtual cavity are about $500 \times 350 \times 400\,\text{mm}^3$.

First, we consider the standard way of using the method, in which pressure is measured on all virtual surfaces but not on the source surface. In this case, the comparison of conditioning number versus frequency is presented in Fig. 4. The analysis shows that the impedance matrix is ill-conditioned. The conditioning number decreases globally with frequency and peaks can be seen on the resonance frequencies of the cavity. To clarify this tendency, we consider a second situation corresponding to the first, but with the addition of a pressure measurement on the source surface.

The conditioning number, presented in Fig. 4, clearly indicates that the impedance matrix is better conditioned. Pressure information on the source surface is therefore important for decreasing the conditioning number. Unfortunately, measuring pressure on the source surface is not often possible in reality. However, it may be sufficient to measure only a few pressure data on the source surface in order to effectively decrease the conditioning number. In this way, we assume that pressure is measured on all the virtual surfaces and on only one patch located in the center of source surface. The result is presented in Fig. 4 with one additional pressure point on the source surface. Above 1200 Hz, the conditioning number is divided by two which represents a real improvement. However, at a lower frequency, no significant modifications of the conditioning number appear.

2.4.2. Influence of the number of pressure control points

From a practical point a view, one may ask whether all the pressure information on the virtual surfaces is necessary. To this end, we used the same source geometry and virtual cavity as in Section 2.4.1, but only used the pressure information measured on the top virtual surface (see Fig. 3), instead of using the pressure information on all the virtual surfaces. Conditioning numbers versus frequency are presented in Fig. 5 for the previous situations. As expected, the analysis shows that it is preferable to measure the pressure field on all the virtual surfaces to limit the conditioning number.

Thus the conclusion is simple: the greater the number of patch pressure measurements, the lower the conditioning number. Practically, it is recommended to measure pressure and velocity data on all the patches of the virtual surface and if possible on additional points on the source surface. In the rest of this paper, pressure information on the source surface is voluntarily not measured since the aim is to find a method for identifying source velocity well without measuring data on the source surface.

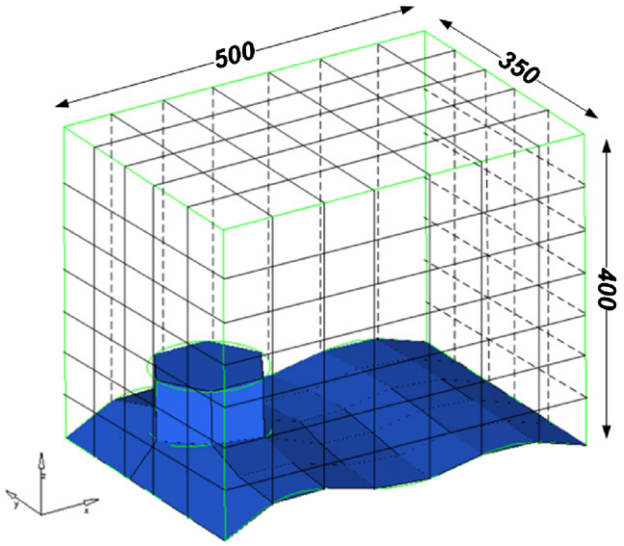

Fig. 3. Geometry of the vibrating source and patch mesh definition on the surface of the virtual cavity.

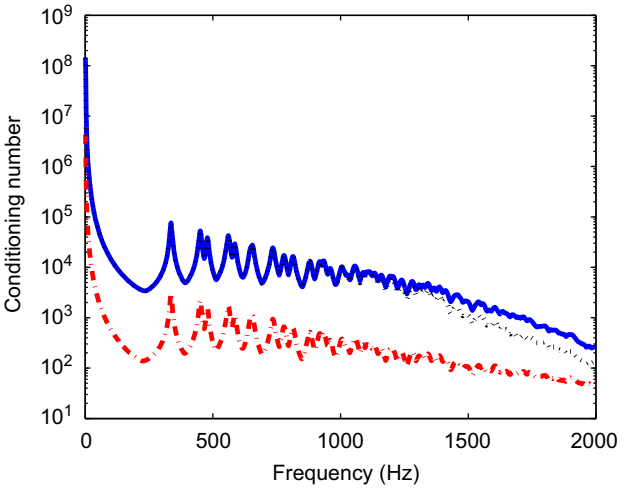

Fig. 4. The conditioning number of patch impedance matrices—comparison between (-) pressure measured on all the virtual surfaces, (-.-) pressure measured on all the virtual surfaces and on the source surface and (- -) pressure measured on all the virtual surfaces and on one patch located in the center of source surface.

2.4.3. Influence of virtual cavity dimensions

In the iPTF method, the virtual cavity can be defined arbitrarily. It is therefore interesting to know whether it is preferable to perform measurements on a small or large virtual cavity. To compare the results, we consider the same source geometry as in the previous subsection (see Fig. 6). The virtual cavity smaller than the previous one is almost a parallelepiped with dimensions about $500 \times 350 \times 120\,\text{mm}^3$ and the patch mesh is defined on virtual surfaces as presented in Fig. 6. Furthermore, we assumed that pressure and particle velocity are measured on all the virtual surfaces.

Fig. 7 presents conditioning numbers for large and small virtual cavities (see Figs. 3 and 6). This figure shows that the patch impedance matrix conditioning number for a small cavity is better at low frequency than that obtained for a large cavity. However, when modal overlap is achieved both cavities have similar conditioning numbers. A small cavity is therefore preferable to limit the conditioning number. This point can be associated with the well-known need with holographic methods for measurements to be made in the nearfield of the source due to the evanescent nature of the acoustic nearfield.

2.4.4. Influence of virtual cavity modes

Ill-conditioning can also be due to poor definition of the virtual volume and patch mesh. Ouisse et al. [16] define a numerical criterion to limit the ill-conditioning of patch impedance matrices. This criterion stipulates that the order of

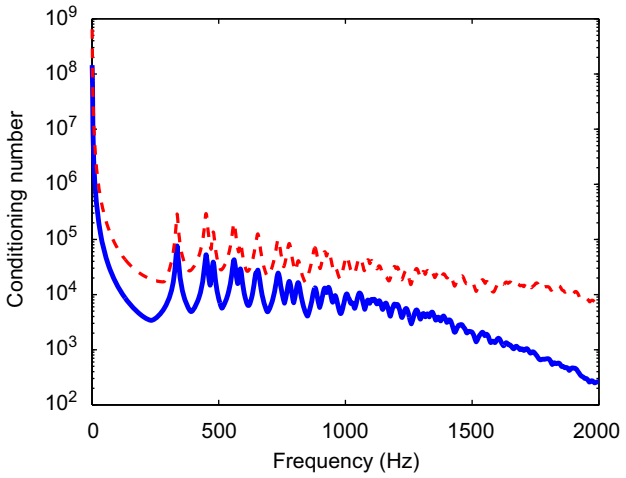

Fig. 5. Conditioning number of patch impedance matrices—comparison between (-) pressure measured on all the virtual surfaces and (- -) pressure measured on the top virtual surface.

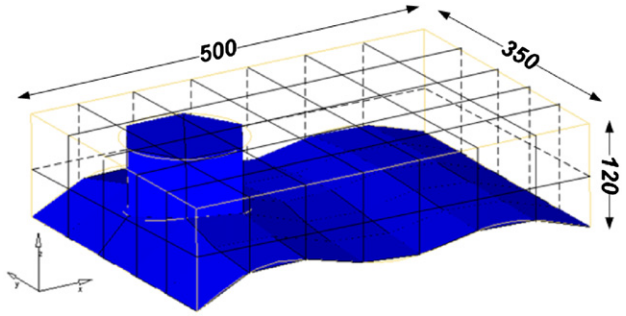

Fig. 6. Geometry of the vibrating source and patch mesh definition on the surface of a $500 \times 350 \times 120\,\mathrm{mm}^3$ virtual cavity.

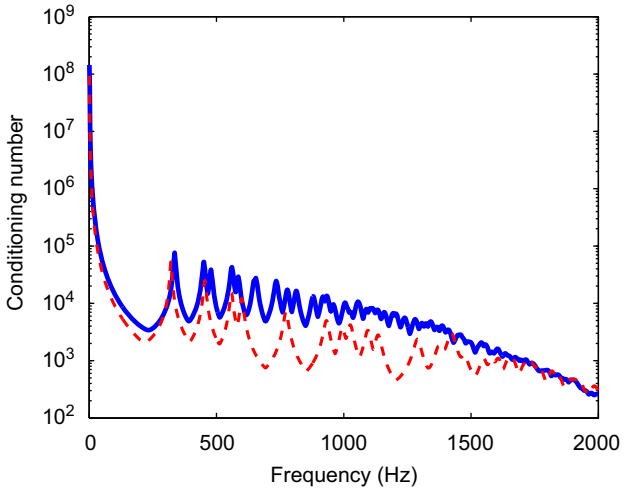

Fig. 7. Conditioning number of patch impedance matrices—comparison between pressure–velocity measured on all the virtual surfaces for (-) the large virtual cavity and (- -) the small virtual cavity.

virtual cavity modes in one direction has to be greater than or equal to the number of patches in the same direction. It corresponds in fact to the number of degrees of freedom necessary to ensure that patch motions are independent. To demonstrate the validity of this criterion, the conditioning number is evaluated for a parallelepiped virtual cavity whose dimensions are $450 \times 350 \times 130\,\mathrm{mm}^3$. A patch mesh is then defined on the measurement and source surface and natural

modes were extracted up to 2, 3, 4 and 5 kHz. In each case, patch impedance matrices were computed in the frequency range of interest [10, 2000 Hz]. As shown in Table 1, the criterion is not respected for modes extracted up to 2 kHz; consequently, the patch impedance matrix is extremely ill-conditioned (see Fig. 8). Furthermore, the criterion is respected above 3 kHz and conditioning numbers are very much better than those obtained for modes extracted up to 2 kHz.

This criterion is not directly applicable when the geometry of the virtual cavity is complex. However, the number of virtual cavity modes must be at least equal to the number of patches.

3. Numerical and experimental validation of the iPTF method

In this section, we seek to validate the iPTF method numerically and experimentally from a simple set-up. The selected set-up consists of two baffled pistons driven in antiphase as shown in Fig. 9. The chosen test case is voluntarily simplified in order to clearly establish how the method is able to localize and separate vibrating sources. The identification area (dimensions: $450 \times 350\,\text{mm}^3$) is divided into 30 patches where pressure and particle velocity are assumed to be constant. Furthermore, the patch impedance matrices computed in this validation section are sufficiently well conditioned to avoid the use of regularization techniques.

Table 1
Comparison between the maximal order of cavity modes and the number of patches along directions x, y and z.

Modal frequency limit (kHz)	2	3	4	5
Maximal order of modes	$5 \times 4 \times 1$	$7 \times 6 \times 2$	$10 \times 8 \times 3$	$13 \times 10 \times 3$
Number of measurement patches	$6 \times 5 \times 2$			
Number of source patches	6×5			

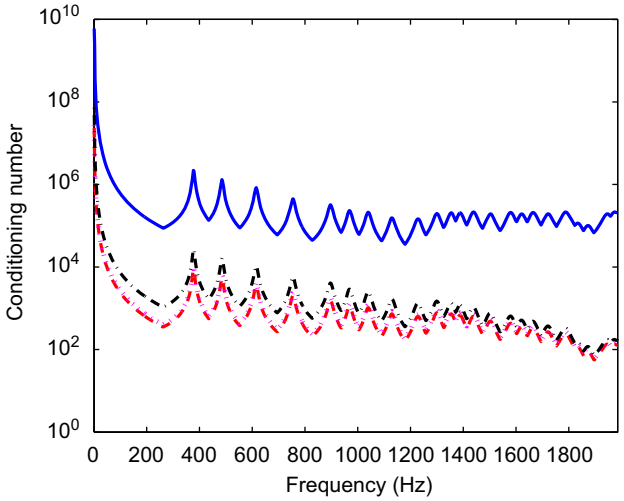

Fig. 8. Influence of the maximal order of cavity modes on the conditioning number of patch impedance matrices for a $450 \times 350 \times 130\,\text{mm}^3$ virtual cavity and modes extracted up to (-) 2 kHz, (- -) 3 kHz, (..) 4 kHz and (-.-) 5 kHz.

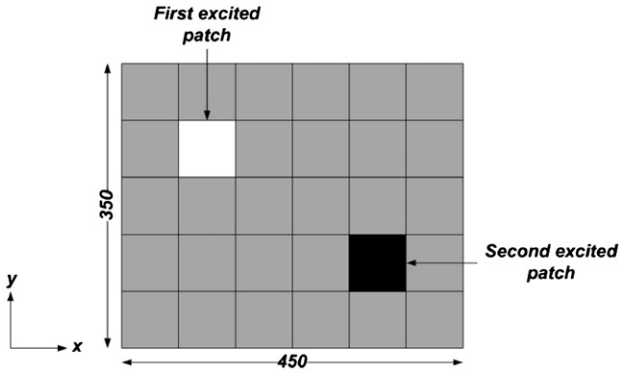

Fig. 9. Definition of the validation set-up—two baffled pistons driven in antiphase.

3.1. Numerical validation

3.1.1. Validation of the basic principle

To validate the basic principle given by Eq. (11), we define a parallelepiped virtual cavity $450 \times 350 \times 20\,\text{mm}^3$ around the source (see Fig. 10a). Moreover, in the PTF method, the definition of patch meshes is driven by a wavelength criterion according to Ouisse et al. [16]. They have demonstrated that in its direct formulation, the PTF method is applicable with a $\lambda_{ac}/2$ criterion for patch meshes. However, for the iPTF method, an additional condition must be considered, i.e. the measurement mesh has to be fine enough to obtain a sufficient number of measurement data. In other words, the number of measurement patches has to be larger than the number of identification patches to avoid under-determination of the problem. Based on this observation, the measurement surface is divided into 139 patches and pressure and particle velocity fields are computed analytically at the center of each measurement patch with the standard Rayleigh integral method (see Appendix B for details).

The process allows good identification of the source velocity, since there is a slight difference between the reference and identification maps at 240 Hz, as shown in Figs. 11 and 12.

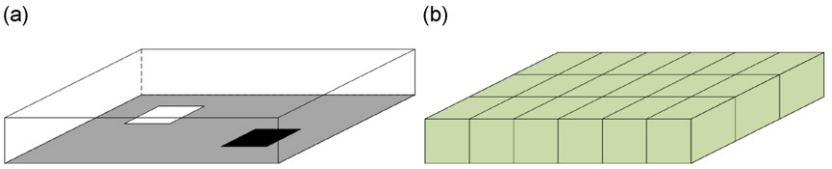

Fig. 10. Definition of (a) the virtual cavity and (b) the patch mesh around the source.

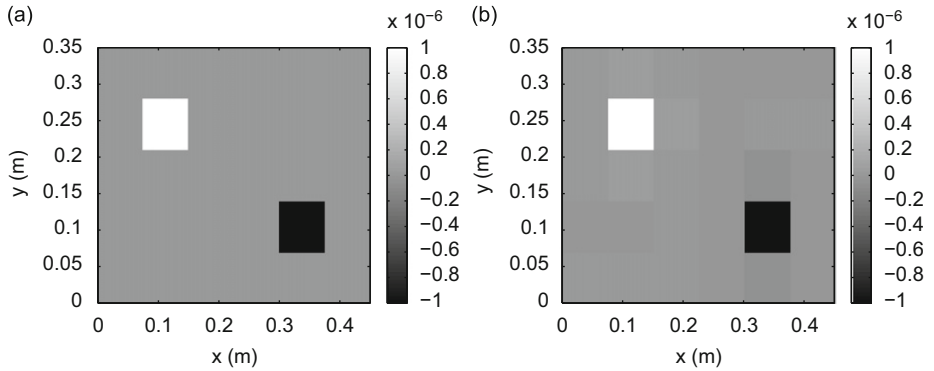

Fig. 11. Numerical validation for a $450 \times 350 \times 20\,\text{mm}^3$ virtual cavity—comparison of (a) the reference map and (b) the identified map obtained with the iPTF method at 240 Hz.

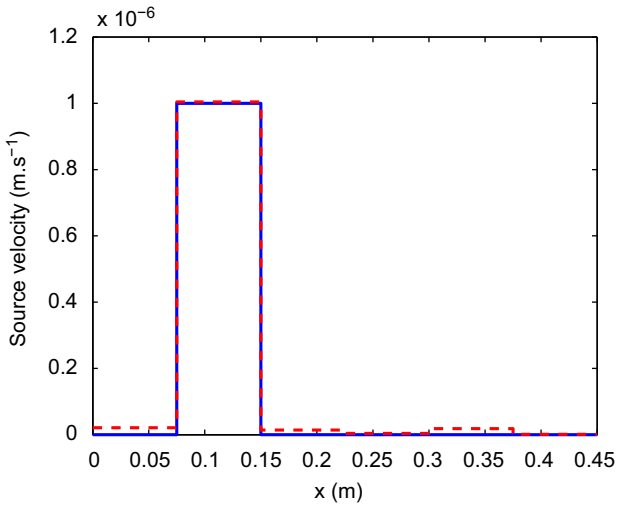

Fig. 12. Numerical validation for a $450 \times 350 \times 20\,\text{mm}^3$ virtual cavity—comparison of source velocity along a line (x, 0.245 m) across the prediction plane at 240 Hz, (-) reference, (- -) identification.

3.1.2. Robustness of the iPTF method—influence of the measurement noise

Measurement noise is an important parameter in result accuracy. In order to analyse the influence of measurement uncertainties, we propose slightly modifying the exact pressure and particle velocity fields computed analytically by introducing two independent Gaussian random variables ΔQ and $\Delta\phi$, that simulate errors on the magnitude and phase of the measurement data [20]:

$$\begin{cases} \tilde{P} = P^{\text{exact}}.\Delta Q_p.e^{j\Delta\phi}, \\ \tilde{V} = V^{\text{exact}}.\Delta Q_p.e^{j\Delta\phi}, \end{cases} \tag{16}$$

where $\Delta Q_p = p|P^{\text{exact}}|X+1$ and $\Delta\phi = \arctan(p)Y$, with p are the noise percentage while (X, Y) are two independent Gaussian random variables.

Figs. 13 and 14 show the influence of measurement uncertainties on identifications for p=30%. It can be seen that measurement noise has a limited influence on identification accuracy, insofar as the magnitude and spatial distribution of source velocities are affected only marginally. Consequently, the proposed method appears to be robust with respect to measurement uncertainties.

3.2. Robustness of the iPTF method—influence of correlated disturbing source

When performing measurements in situ, correlated sources can modify the pressure and the particle velocity fields measured around the source to be identified. Consequently, virtual sources are likely to appear on the hologram due to the bad estimation of the acoustic field in the measurement area. As underlined in Section 2, the iPTF method is theoretically independent of the presence of external sources. To prove this theoretical aspect, a third piston is inserted in the rigid

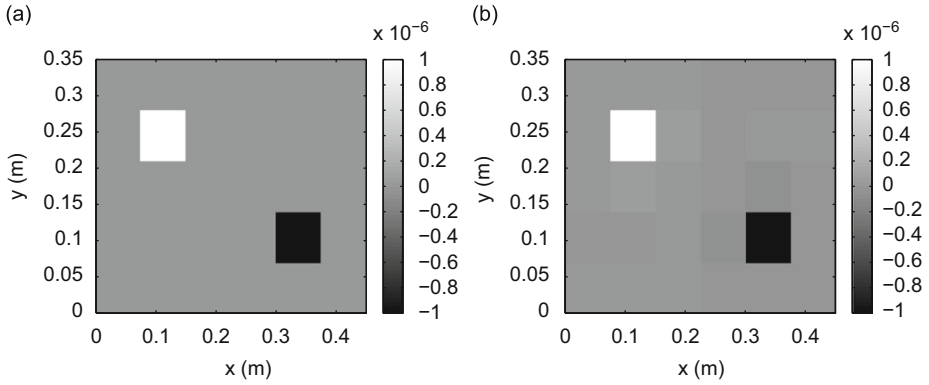

Fig. 13. Numerical validation for a $450 \times 350 \times 20\,\text{mm}^3$ virtual cavity—comparison between (a) the reference map and the identified maps obtained for (b). (b) p=30% at 240 Hz.

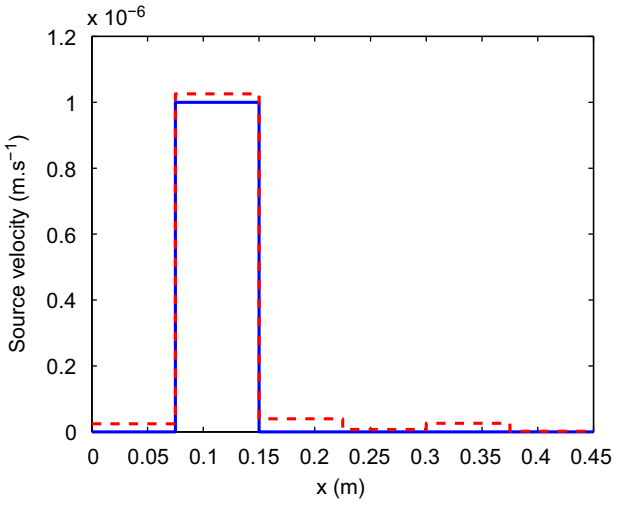

Fig. 14. Numerical validation for a $450 \times 350 \times 20\,\text{mm}^3$ virtual cavity—comparison of the source velocity along a line (x, 0.245 m) across the prediction plane at 240 Hz, (-) reference, (- -) identification for p=30%.

baffle, where the velocity is 5 times greater than that of the first piston (see Fig. 15). This third disturbing piston modifies the acoustic field computed at the center of the measurement patches. As an example, the mean square pressure is increased by 6.5 dB at 240 Hz, while the mean square particle velocity is increased by 3.5 dB at the same frequency.

Fig. 16 presents the comparison of the spatial distribution of reference source velocity with the identified source velocity obtained in the presence of a disturbing acoustic source. The maps prove that the source velocity can be well identified in the presence of a disturbing source (Fig. 17).

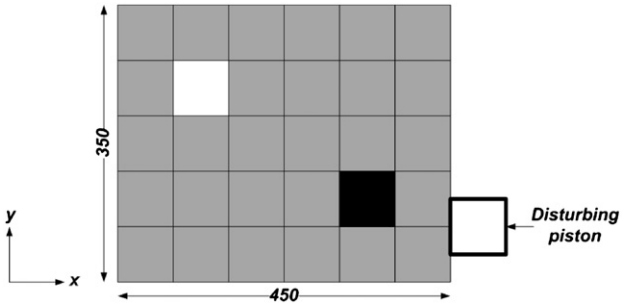

Fig. 15. Location of the disturbing piston outside the identification area.

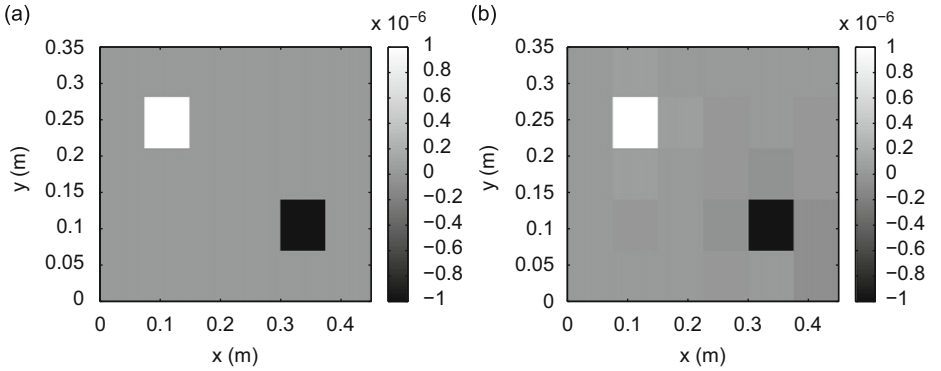

Fig. 16. Numerical validation for a $450 \times 350 \times 20\,\text{mm}^3$ virtual cavity in the presence of an external disturbing source—comparison of (a) the reference map and (b) the identified map obtained at 240 Hz.

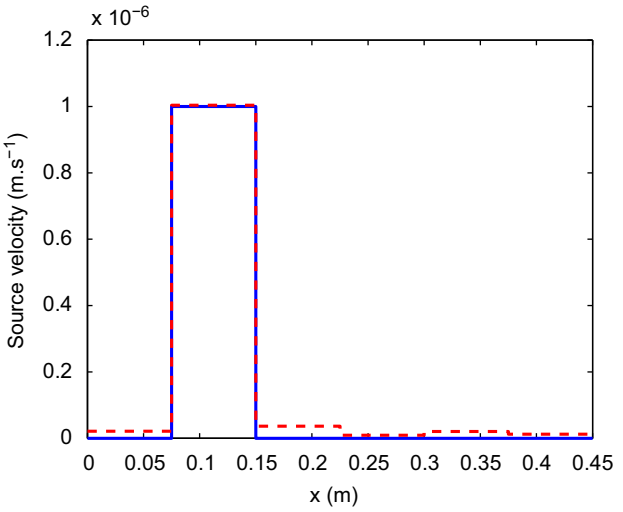

Fig. 17. Numerical validation for a $450 \times 350 \times 20\,\text{mm}^3$ virtual cavity in the presence of an external disturbing source—comparison of source velocity along a line (x, 0.245 m) across the prediction plane at 240 Hz, (-) reference, (- -) identification.

3.2.1. Influence of the virtual cavity dimensions

The dimensions of the virtual cavity are essential in the identification process since the further the measurement is made from the source, the greater the loss of near field information related to the evanescent waves. In this case, it is hard to identify the source velocity precisely due to the lack of information. To demonstrate the influence of the cavity dimensions on identification, we define a virtual cavity whose dimensions are $450 \times 350 \times 130\,\text{mm}^3$. Furthermore, the measurement surface is divided into 259 patches. As shown in Fig. 18, the iPTF method identifies the source velocities successfully. However, as classically observed in other holographic methods (NAH or iBEM), source localization and separation are less clear because of the absence of near field information in the data considered.

3.3. Experimental validation

3.3.1. Experimental set-up

The experimental validation consists in reproducing as reliably as possible the set-up used for the numerical validation in order to evaluate the applicability and the robustness of the method in a non-anechoic environment. To do this, the acoustic baffle consists of a thick wooden plate $700 \times 600 \times 40\,\text{mm}^3$, in which two loudspeakers supplied by white noise are inserted. Furthermore, the identification area is materialized on the rigid baffle as shown in Fig. 19. It can also be seen that the measurements were performed in a non-anechoic chamber and thus included sound reflected from room boundaries. Finally, reference and acoustic field measurements were carried out with a PU probe in the very nearfield of the source (5 mm from the acoustic source) and a microphone was used as phase reference.

As in the previous sections, we defined the same patch meshes around the identification area as those used in the numerical validation. It should be recalled that the space averaged data of the pressure and particle velocity on the patches

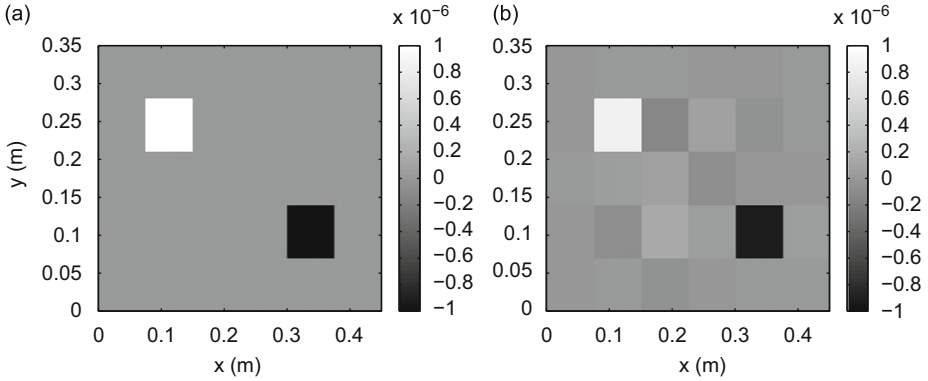

Fig. 18. Numerical validation for a $450 \times 350 \times 130\,\text{mm}^3$ virtual cavity—comparison between (a) the reference map and (b) the identified map obtained with the iPTF method at 240 Hz.

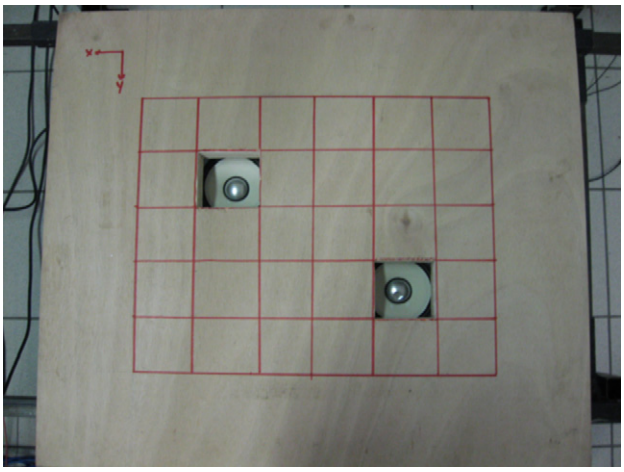

Fig. 19. Experimental set-up.

are represented by one measurement point at the center of the patch. Therefore a positioning error of the PU probe can influence the quality of the experimental results. Of course, other factors can be involved such as the orientation of normal vectors for particle velocity measurements or uncertainties due to transducer quality.

In the following, we use an indicator ε which allows thorough determination of the identification error of the iPTF method. This indicator is defined in

$$\varepsilon = 10\log\left|\frac{V_{\mathrm{id}}^2}{V_{\mathrm{ref}}^2}\right|, \tag{17}$$

where V_{ref} is the source velocity measured in the very nearfield of the source and V_{id} is the identified source velocity.

3.3.2. Validation of the basic principle

The experimental validation of the basic principle is performed by reproducing the numerical experiment used in Section 3.1. When applying the iPTF method to experimental data, good agreement between the measured and identified source velocity is observed in both magnitude and spatial distribution (see Figs. 20 and 21). Analysis of Fig. 20 shows that the identification error on the first excited patch ((x, y)=(0.1125, 0.245 m)) does not exceed 0.7 dB over the entire frequency range.

3.3.3. Robustness of the iPTF method—influence of correlated disturbing source

To test the robustness of the method in the presence of a correlated disturbing source, we used the same virtual cavity as in the previous case and a third loudspeaker located outside the measurement area was added (see Fig. 22). A reference measurement was performed again to take into account the acoustic field modifications due to the disturbing source.

The pressure power spectrum measured on a patch of the measurement surface with and without the disturbing source highlights its influence. Disturbing pressure was in general of the same order as the primary source pressure and at certain frequencies differed by more than 5 dB (see Fig. 23).

The iPTF method allows determining a source velocity whose magnitude differs from the reference by 0.72 dB at most over the entire frequency range, as shown in Fig. 24 which presents the identification error on the first excited patch ((x, y)=(0.1125, 0.245 m)). Moreover, Fig. 25 shows a comparison between the reference map and the identified map. This comparison confirms the ability of the method to reconstruct the spatial source velocity distribution in the presence of an external stationary disturbing source.

3.3.4. Influence of the virtual cavity dimensions

As already mentioned in the numerical validation of the method, the further from the source the sound field is measured, the greater the loss of information related to the evanescent waves. The aim of this section is to determine experimentally how the absence of near field information affects identification accuracy. To achieve this, we use the virtual cavity with dimensions $450 \times 350 \times 130\,\mathrm{mm}^3$ defined in Section 3.2.1. Once again the iPTF method gives quite satisfying results in both magnitude and spatial distribution (see Figs. 26 and 27). However, Fig. 26 shows that identification is less accurate in magnitude than that performed on a cavity of smaller dimensions. However, the discrepancy is acceptable up

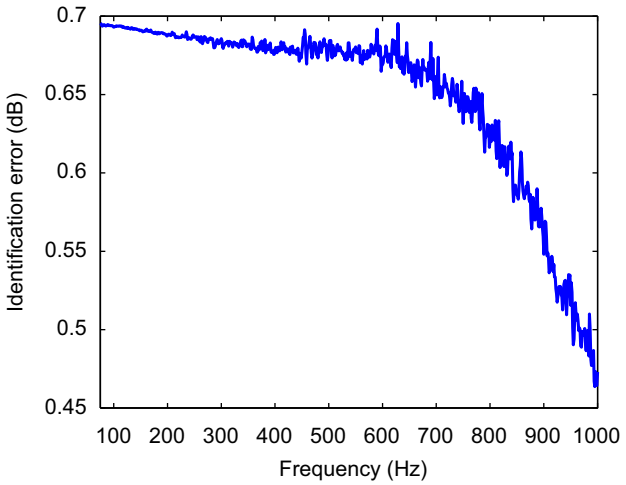

Fig. 20. Experimental validation for a $450 \times 350 \times 20\,\mathrm{mm}^3$ virtual cavity—identification error on the first excited patch (x, y)=(0.1125, 0.245 m).

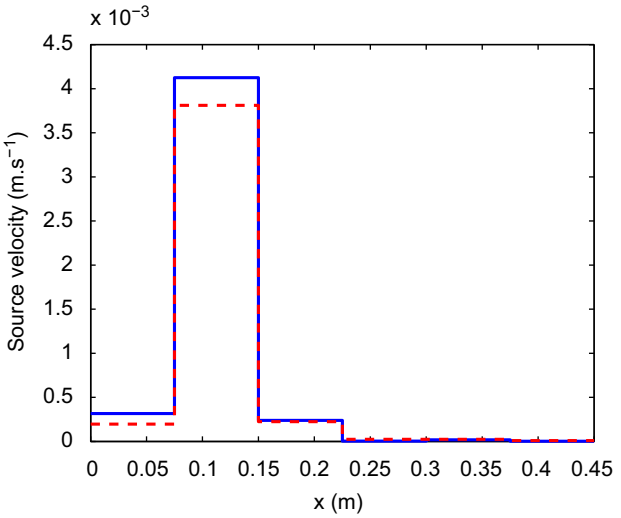

Fig. 21. Experimental validation for a $450 \times 350 \times 20\,\text{mm}^3$ virtual cavity—comparison of source velocity along a line (x, 0.245 m) across the prediction plane at 240 Hz, (-) reference, (- -) identification.

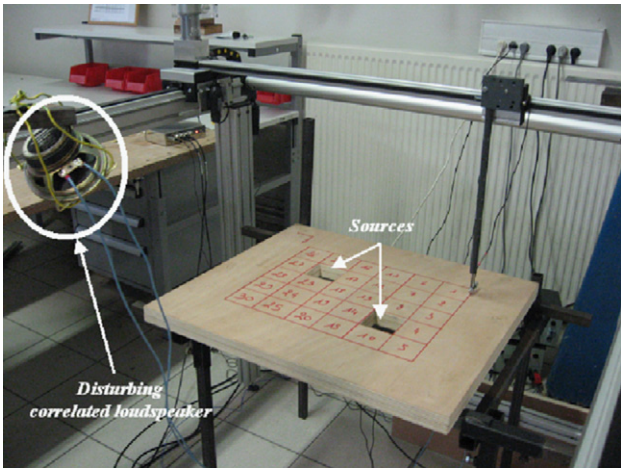

Fig. 22. Experimental set-up—location of the disturbing source.

to 425 Hz, where the height of the virtual cavity reaches $\lambda_{ac}/6$ ($340/6 \times 425 \approx 0.13$ m). Nevertheless, the method succeeds in localizing the two loudspeakers, even if their magnitudes are underestimated.

4. Conclusion

The iPTF method allows identifying source velocities on complex structures. This paper introduced both the theoretical background and the measurement methodology. The method comprises the measurement of the pressure and particle velocity fields on the virtual cavity surfaces. This is quite simple when using PU probes. To prove the method's efficiency, an experimental validation was set up with two baffled pistons driven in antiphase.

As classically observed in holographic methods, one of the main drawbacks remains the loss of near field information when measuring an acoustic field far from the source.

However, the combined use of an integral formulation, FEM as a solver and the double measurement of pressure and particle velocity fields overcomes some of the limitations of classical methods related to simple structure geometry. Thus, the main advantages of the iPTF method are its independence with respect to external stationary sources and its applicability to complex shaped structures. Finally, further applications of the method on more complex structures than that presented in this article, namely an L-shape plate and a vehicle precatalyst, can be found in Refs. [21,22].

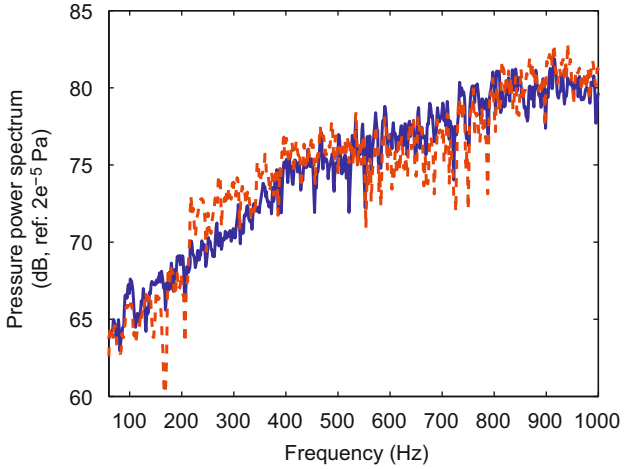

Fig. 23. Comparison between the pressure power spectrum obtained on a patch of the measurement surface (-) without and (- -) with the disturbing source versus frequency.

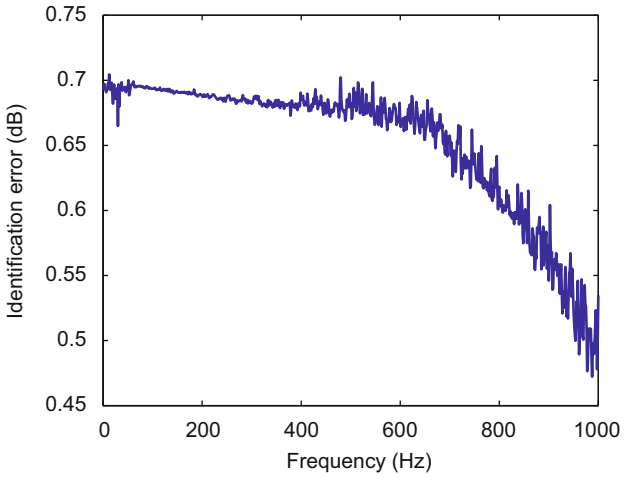

Fig. 24. Experimental validation for a $450 \times 350 \times 20\,\text{mm}^3$ virtual cavity in the presence of an external correlated disturbing source—identification error on the first excited patch (x, y)=(0.1125 m, 0.245 m).

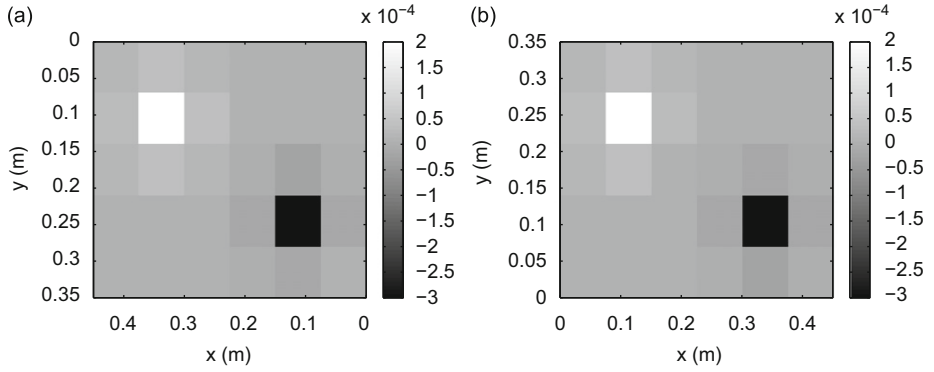

Fig. 25. Experimental validation for a $450 \times 350 \times 20\,\text{mm}^3$ virtual cavity in the presence of an external correlated disturbing source—comparison between (a) the reference map and (b) the identification map obtained experimentally in the presence of a disturbing source with the iPTF method at 240 Hz.

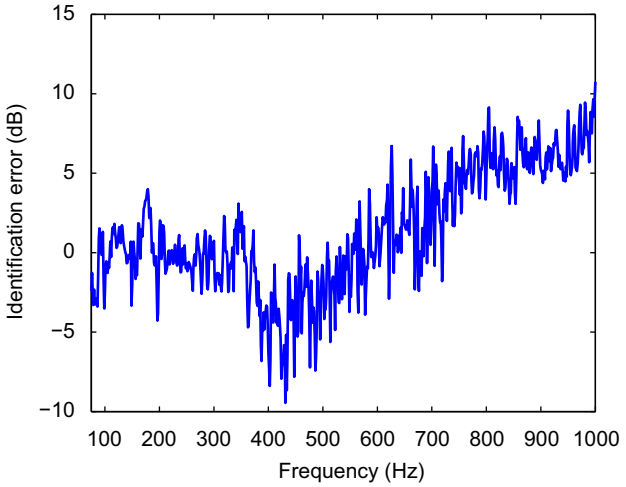

Fig. 26. Experimental validation for a $450 \times 350 \times 130\,\mathrm{mm}^3$ virtual cavity—identification error on the first excited patch (x, y)=(0.1125, 0.245 m).

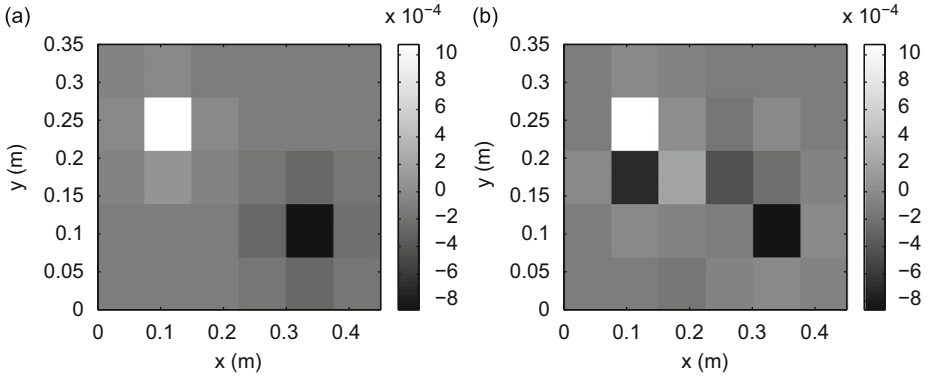

Fig. 27. Experimental validation for a $450 \times 350 \times 130\,\mathrm{mm}^3$ virtual cavity—comparison between (a) the reference map and (b) the identified map obtained experimentally with the iPTF method at 240 Hz.

Appendix A. Calculation of Green's function by a modal approach

The Green's identity defined in Eq. (2) is then used, Φ is the mode shape ϕ_n of the virtual rigid cavity wall Ω_c satisfying Eq. (18) and Ψ is the function G satisfying Eq. (4):

$$\begin{cases} \Delta\phi_n(M) + k_n^2\phi_n(M) = 0, & \forall M \in \Omega_c, \\ -\dfrac{1}{\mathrm{j}\rho\omega}\dfrac{\partial\phi_n}{\partial n}(Q) = 0, & \forall Q \in S_c. \end{cases} \tag{18}$$

Consequently, by using Eqs. (2), where $\Phi = \phi_n$ and $\Psi = G$, (4) and (18), we obtain the integral equation given by

$$\phi_n(Q') = \iiint_{\Omega_c} (k_n^2 - k^2)\phi_n(M)G(M,Q')\,\mathrm{d}M. \tag{19}$$

The function G is now determined by expansion on the modal basis $\phi_n(M)$:

$$G(M,Q') = \sum_n g_n(Q')\phi_n(M). \tag{20}$$

Using this decomposition in Eq. (19), one obtains:

$$g_n(Q') = \frac{c^2\phi_n(Q')}{\Lambda_n(\omega_n^2 - \omega^2)}, \tag{21}$$

where the norm of modes is such that $\iiint_{\Omega_c}\phi_n(M)\phi_q(M)d\Omega_c = \Lambda_n\delta_{nq}$. Therefore the following expression is obtained:

$$G(M,Q') = \sum_n \frac{c^2\phi_n(M)\phi_n(Q')}{\Lambda_n(\omega_n^2 - \omega^2)}. \tag{22}$$

The patch impedance between a source patch k and a reception patch j is therefore:

$$Z_{jk} = -\sum_n \frac{j\omega\rho c^2 S_k}{\Lambda_n(\omega_n^2-\omega^2)} \overline{\phi_{n_k}}\ \overline{\phi_{n_j}}. \tag{23}$$

Obviously, in Eqs. (22) and (23), this modal composition caused problems at resonant frequencies. To avoid these difficulties, we introduce the modal damping of fluid η_n, which is a constant in this study. Therefore, the term $\omega_n^2-\omega^2$ by the term $\omega_n^2-\omega^2+j\eta_n\omega_n\omega$ is replaced in the denominator.

Appendix B. Radiation of a baffled piston

The Rayleigh integral formulation of a baffled piston is used to compute its radiation as expressed in

$$\begin{cases} p(M) = -j\rho\omega\int_S V(Q)G(M,Q)\,dQ, \\ G(MQ) = \dfrac{e^{-jkR}}{2\pi R}, \end{cases} \tag{24}$$

$$V(Q) = \begin{cases} \overline{V}_n, & \forall Q \in S_{\text{piston}}, \\ 0 & \text{elsewhere}. \end{cases} \tag{25}$$

However, insofar as the dimension of the piston is not negligible, the integral over the piston area is discretized into $n_x \times n_y$ points. Consequently, Eqs. (24) and (25) become:

$$\begin{cases} p(M_r) = j\rho\omega\overline{V}_n\sum_k \dfrac{e^{-jkR_{kM_r}}}{2\pi R_{kM_r}}\Delta x_k \Delta y_k \\ R_{kM_r} = \sqrt{(x_{M_r}-x_k)^2+(y_{M_r}-y_k)^2+(z_{M_r}-z_k)^2} \end{cases}, \tag{26}$$

where $(x_{M_r}, y_{M_r}, z_{M_r})$ are the coordinates of the center of the patch r and (x_k, y_k, z_k) are the coordinates of the point k belonging to the piston.

The particle velocity is then easily obtained at the center of the patch r by using the Euler's equation defined in

$$V(M_r) = -\frac{1}{j\rho\omega}\frac{\partial p}{\partial n_e}(M_r), \tag{27}$$

where n_e is the external normal vector to the virtual cavity.

References

[1] E.G. Williams, J.D. Maynard, E. Skudrzyk, Sound source reconstructions using a microphone array, *Journal of the Acoustical Society of America* 68 (1980) 340–344.

[2] E.G. Williams, The nearfield acoustical holography (NAH) experimental method applied to vibration and radiation in light and heavy fluids, *Computers & Structures* 65 (3) (1997) 323–335.

[3] E.G. Williams, The inverse problem: planar nearfield acoustical holography, in: *Fourier Acoustics: Sound Radiation and Nearfield Acoustical Holography*, Academic Press, London, 1999, pp. 89–114 (Chapter 3).

[4] E.G. Williams, The inverse problem: cylindrical NAH, in: *Fourier Acoustics: Sound Radiation and Nearfield Acoustical Holography*, Academic Press, London, 1999, pp. 149–182 (Chapter 5).

[5] E.G. Williams, Spherical nearfield acoustical holography, in: *Fourier Acoustics: Sound Radiation and Nearfield Acoustical Holography*, Academic Press, London, 1999, pp. 235–249 (Chapter 7).

[6] B.K. Bai, J.G. Ih, On the reconstruction of the vibro-acoustic field over the surface enclosing space using the boundary element method, *Journal of Acoustical Society of America* 100 (1996) 3003–3016.

[7] F. Martinus, An advanced noise source identification technique using the inverse boundary-element method, *Journal of Acoustical Society of America* 118 (3) (2005) 1916.

[8] S.F. Wu, Hybrid nearfield acoustical holography, *Journal of Acoustical Society of America* 115 (2004) 207–217.

[9] X. Zhao, S.F. Wu, Reconstruction of vibro-acoustic fields using hybrid nearfield acoustic holography, *Journal of Sound and Vibration* 282 (3) (2004) 1183–1199.

[10] S.F. Wu, J. Yu, Reconstructing interior acoustic pressure field via Helmholtz equation least-squares method, *Journal of Acoustical Society of America* 104 (1998) 2054–2060.

[11] N.E. Rayess, S.F. Wu, Experimental validations of the Hels method for reconstructing acoustic radiation from a complex vibrating structure, *Journal of Acoustical Society of America* 107 (2000) 2955–2964.

[12] S.F. Wu, X. Zhao, Combined Helmholtz equation least-squares method for reconstructing acoustic radiation from arbitrarily shaped objects, *Journal of Acoustical Society of America* 112 (2002) 179–188.

[13] Q. Leclère, B. Laulagnet, An alternative acoustic imaging technique to improve capabilities of microphone array measurements, *Proceedings of November 2005*, St. Raphael, France, 2005.

[14] Q. Leclère, B. Laulagnet, L. Polac, Application of an innovative acoustic imaging technique to assess acoustic power maps of a gasoline engine, *Proceedings of Forum Acusticum 2005*, Budapest, Hungary, 2005.

[15] L. Maxit, C. Cacciolati, J.L. Guyader, Airbone noise prediction using patch acoustic impedance, *Proceedings of ICSV9*, Orlando, United States, 2002.

[16] M. Ouisse, L. Maxit, C. Cacciolati, J.L. Guyader, Patch transfer functions as a tool to couple linear acoustic problems, *Journal Vibration Acoustics, Transactions of the ASME* 127 (2005) 458–466.

[17] N. Totaro, B. Andro, C. Peteul, J.L. Guyader, Extension of the Patch transfer functions method (PTF Method) to high frequency domain (sub-cavities decomposition), *Proceedings of Inter-Noise*, Istanbul, Turkey, 2007.

[18] F. Jacobsen, V. Jaud, A note on the calibration of pressure–velocity sound intensity probes, *Journal of Acoustical Society of America* 120 (2) (2006) 830–837.
[19] F. Jacobsen, V. Jaud, Statistically optimized near field acoustic holography using an array of pressure–velocity probes, *Journal of Acoustical Society of America* 121 (3) (2007) 1550–1558.
[20] C. Pezerat, J.L. Guyader, Two inverse methods for localization of external sources exciting a beam, *Acta Acustica* 3 (1995) 1–10.
[21] M. Aucejo, N. Totaro, J.-L. Guyader, Identification of source velocities with iPTF (inverse patch transfer functions method), *Proceedings of Acoustics08*, Paris, France, 2008.
[22] N. Totaro, C. Sandier, J.-L. Guyader, Identify velocity of a complex source with iPTF method, *Proceedings of ICSV15*, Daejon, South Korea, 2008.